Ocean Sci. Discuss., 12, 83–101, 2015
www.ocean-sci-discuss.net/12/83/2015/
doi:10.5194/osd-12-83-2015

Ocean Science
Discussions
Open Access

Sea surface height and mixed layer depth responses to sea surface temperature in northwestern Pacific subtropical front zone from spring to summer

C. Qiu[1,4], H. Kawamura[2], H. Mao[3], and J. Wu[1]

[1]Center for Coastal Ocean Science and Technology, School of Marine Sciences, Sun Yat-sen University, Guangzhou 510275, China
[2]Center for Atmospheric and Oceanic Studies, Graduate school of Science, Tohoku University, Japan
[3]State key Laboratory of Tropical Oceanography, South China Sea Institute of Oceanology, Chinese Academy Science, China
[4]Guangdong Provincial Key Laboratory of Marine Resources and Coastal Engineering, School of Marine Sciences, Sun Yat-sen University, Guangzhou, China

Received: 24 December 2014 – Accepted: 11 January 2015 – Published: 21 January 2015

Correspondence to: J. Wu (wujiaxue@mail.sysu.edu.cn)

Published by Copernicus Publications on behalf of the European Geosciences Union.

Abstract

Qiu et al. (2014) quantitatively examined the mechanisms of sea surface temperature front disappearance, finding that the formation of shallow mixed layer depth (MLD) is very important. In the present study, we further investigated variations of the sea level anomaly (SLA) and mixed layer depth (MLD) during the SST front weakening period, based on weekly satellite derived products. For the SLA, we examined the steric height component of SLA, using empirical orthogonal function (EOF) method and physical method. The seasonal variations of steric height from above two methods have the same pattern: peak value (~ 20 cm) occurs in July-August, and minimum value (~ −5 cm) occurs in February to March. Correlation between SLA and SST achieves 0.76 in cold zone and frontal zone, and it is 0.86 between steric component and SST. When SST becomes large, MLD decreases gradually. The linear relationship ($y = -4.46x + 156.47$) between MLD and SST could be used to estimate the MLD in the subtropical front zone.

1 Introduction

The subtropical front is one of the major oceanic features of the North Pacific, separating the warm saline North Pacific Central waters in the south from the cool fresh waters to the north. Sea surface temperature (SST) front modulates the atmospheric conditions, such as wind speed magnitude and wind directions (e.g., Xie, 2004; Small et al., 2008), temperature, turbulent fluxes (Friehe et al., 1991), and deep atmospheric responses (Kobashi et al., 2008). All of them differ significantly from one side of an SST front to the other, with an increase (decrease) in wind speed as the wind blows from cold (warm) to warm (cold) water across the front (Friehe et al., 1991).

Subtropical SST front were suggested to be accompanied with mixed layer depth (MLD) and sea surface height (SSH) (e.g., Uda and Hasunuma, 1969; White et al., 1978; Qiu and Lucas, 1996; Qiu, 2002; Kobashi et al., 2008; Kobashi and Xie, 2012; Kobashi and Kubokawa, 2012) Qiu et al. (2014) quantitatively examined the mechanisms of subtropical SST front in April to September, and confirmed the air-sea heat exchanging induces the subtropical SST front disappearance. They also found the geotropic advection calculated from the gradient of SSH, was quite small compared with net heat flux. Although the SSH gradient magnitude were small, the SSH in this area (130–160° E, 20–32° N) has relatively large meso-scale variability (Kobashi and Kawamura, 2001). How the SSH vibrates needs to be examined more clearly in the SST front zone.

Nonlinear relationship between net heat flux and MLD were found to be very important during the SST front weakening period (Qiu et al., 2014). As known to us, oceanic MLD is primarily determined by the action of turbulent mixing of the water mass due to wind stress and heat exchange at the air-sea interface (Kara et al., 2003). MLD is associated with the SSH variation, because SST cooling could induce convection, and convection result in MLD enlarge, and also induce SSH decrease (e.g. Monterey and Levitus, 1997; de Boyer Montegut et al., 2004). But atmospheric condition, wave and eddy also contribute to the SSH (Stammer, 1997). We need to check the relationship between SSH / MLD and SST carefully.

In the present study, we investigate the upper-layer changes based on 7 years weekly products of AMSR-E SSTs, altimeter data and in situ observations in northwestern subtropical area. We pay attention to (1) the seasonal variation of the SST front evolution; (2) relationship between SST, sea surface height and the mixed layer depth. The data and methods are described in Sect. 2. Results and discussions are given in Sect. 3. Section 4 is the summary.

2 Data and methods

The Advanced Microwave Scanning Radiometer (AMSR) for the Earth observing system (AMSR-E) on the Aqua satellite has provided global observations of SST since 2003. We use AMSR-E level 2 data from 1 January 2003 to 31 December 2009.

OSD
12, 83–101, 2015

The original spatial resolution is around 10 km, we interpolated the products into 0.125° × 0.125°. Every day two snap images were used. The data processing is directed to Qiu and Kawamura (2012). The availability of AMSR-E has no apparent seasonal variation in subtropical area (Hosoda, et al., 2010). Therefore, AMSR-E data are good enough to detect the variation of SST front.

Merged sea level anomaly (SLA) data were used. The data came from two satellite missions, TOPEX/Poseidon and ERS, followed by Jason-1 and Envisat. This dataset has stable sampling in time (AVISO, 2006). The mapped altimetry dataset includes one map every 7 days with a (1 / 3)° spatial resolution on a Mercator grid (Ducet et al., 2000).

2003–2009 daily surface flux products are derived from National centers for Environmental Prediction/National center for Atmospheric Research (NCEP/NCAR) reanalysis project. The spatial resolution is 2.5° × 2.5°. We obtained the net heat flux Q by summarized sensible heat net flux, latent heat net flux, net longwave radiation and net shortwave radiation. Here, upward is positive and downward is negative.

To investigate the vertical structure of upper layer, the global Temperature and Salinity Profile Program (GTSPP) "Best Cop" data are used. The data include the full-resolution data from XBTs or CTDs from the ships, or fully processed and quality-controlled data from the organizations that provided the real-time low-resolution data to the GTS (Sun et al., 2010). The data from 1 January 2003 to 30 September 2009 are obtained. The temperature / salinity profile data are firstly interpolated onto 1 m vertical resolution grid, and then density ρ and pressure P for each depth are calculated. The temperature in depth z is written as T_z, and the in situ surface temperature is T_0.

OSD
12, 83–101, 2015

3 Results and discussions

3.1 Seasonal variation of subtropical SST front

Figure 2 shows the seasonal variation of SST front. The frontal strength recognized by SST gradient magnitude was shown in Fig. 2a. In 20–32° N, the SST gradient magnitude has significant seasonal variations, with large gradient magnitude from October to next June, and small value from June to September. The SST front weakening period is from April to September, as suggested by Qiu and Kawamura (2012).

The monthly mean frontal positions were shown in Fig. 2b. In different part, the frontal position has different variations. In the western part (130–135° E), the frontal position has significant seasonal variations; In the middle part (135–150° E), the frontal position is stable throughout the year; in the eastern part (150–160° E), frontal position starts to shift seasonally. The subtropical front meets Kuroshio front in the western part and eastern part, but isolated in the middle part, which might lead to the different seasonality of frontal position (Qiu and Kawamura, 2012).

The 7 year mean frontal position (black thick line) and standard deviation of frontal position (grey shaded area) are shown in Fig. 2c. The mean SST front locates at around 22–28° N, with shifting area ±2. According to the frontal position, we separated this area into cold zone, frontal zone and warm zone. The shaded band like area is defined as the subtropical SST front area. The cold zone locates at the north of front, and warm zone locates to the south of front.

3.2 Sea level variations

3.2.1 EOF analysis

To reveal the variations of SSH, we use an empirical orthogonal function (EOF) analysis. The EOFs account for 26.7, 15.4, 4.5, and 3.6 % of SLA variance for the first-fourth mode, respectively (Fig. 3). Their contributions are relative small compared with that

OSD
12, 83–101, 2015

obtained by Isoguchi et al. (1997), which might result from the study region and study period. The first EOF has sharp height gradient in spatial structures, and its time series represent that the SLA has significant seasonal variations. In summer, the SLA has positive value in cold zone and negative value in warm zone.

We also show the EOF analysis for SST (Fig. 4). The first mode of SSTs has the same spatial pattern (south-high north-low) with that of SLA. It indicates that the first EOF of SLA might explain the steric height component. The second to fourth EOFs preserve many meso-scale eddies, their time series show intera-seasonal variations.

3.2.2 Steric component of SLA

SSH contains several ocean processes, including heating and oceanic current (Stammer, 1997), as shown below,

$$\eta = \eta_{\mathrm{s}} + \eta_{\mathrm{bc}} + \frac{1}{g\rho_0} p_{\mathrm{b}} \tag{1}$$

where η is the SSH, η_{s} is the steric height, η_{bc} is the effect caused by density changes below seasonal thermocline resulting from oceanic currents. The last term stands for the fluctuating of barotropic currents. ρ_0 is the sea water density, c_p is the specific heat of sea water at one constant pressure.

During the SST front weakening period, net heat flux was suggested as the most important component to induce SST variation (Qiu et al., 2014). Therefore, we examine the steric height variation, which caused by heating. Ignoring the freshwater influencing, the steric height anomaly is given by Stammer (1997),

$$\eta_{\mathrm{s}}(\mathrm{t}+1) = \frac{\alpha(\mathrm{t})Q'(t)}{\rho_0 c_p}\Delta\mathrm{t} = \eta_{\mathrm{s}}(\mathrm{t}) \tag{2}$$

then we derived the weekly steric height anomaly, using net heat fluxes anomaly, removing 7-year mean net heat flux. Time-interval is 7 days $\eta_{\mathrm{s}}(0)$ is given by the SLA on

OSD
12, 83–101, 2015

1 January 2003. The thermal expansion coefficient α(t) was evaluated from Table A3.1 of Gill (1982), using Levitus's (1982) mean mixed-layer temperatures. The pressure effect on α(t) was neglected.

Figure 5 shows the seasonal variations of SSH increase ($\partial\eta/\partial t = \eta(t+1) - \eta(t)$), and steric height increase ($\partial\eta_s/\partial t = \eta_s(t+1) - \eta_s(t)$). Their variations are negative in winter (~ −0.5 cm), and increase to maximum value in June–July. The value of $\partial\eta_s / \partial t$ is close to $\partial\eta / \partial t$, in the front zone. It indicates that the steric height leads to the seasonal variation of SSH. In warm zone, the steric height increases a little faster than SSH from March to September in warm zone. But in cold zone, the steric height increases slower than SSH.

We compared the SSHA, the steric height component and the first EOF mode in Fig. 6. Here the EOF mode 1 means the value of spatial pattern multiply the time series in each time. All of them have low value in winter and high value in summer. The peak value (~ 20 cm) of SSH occurs in July, while it is in August for steric height. The steric height and the EOF mode 1 have the same pattern: low value in March and highest value in August; the value has significant changes in north and light change in south. But the steric height seems to the smooth of EOF mode 1st. It might come from the coarse resolution of NCEP/NCAR net heat fluxes. As steric height increases, the SST (solid line in Fig. 4c) also increases quickly.

To examine the relationship between SST and SSH in each field, we match-up the weekly SLA, steric height and AMSR-E SSTs in each grid with 0.125°. Then we obtained the zonal mean data for 7 years. Totally, 365 weeks were derived. The relationship between SST and SSH is shown in Fig. 7. When SST increases from April to September, both the SLA and steric height increase. The correlation between SLA and SST are 0.76, 0.76, 0.38 in cold zone, front zone and warn zone, respectively. For steric height and SST, their correlations are 0.86, 0.84 and 0.79, respectively. In each zones, both the SLA and steric height increase by around 20 cm, although there are some short-term oscillations from April to September (color means in different month).

OSD
12, 83–101, 2015

3.3 Mixed layer depth responses

In examining the SST front disappearance, mixed layer depth (MLD) is very important as $\partial \mathrm{SST} / \partial t \propto -Q/h$ where Q is the net heat flux anomaly, and h is the MLD. Qiu et al. (2014) suggested the nonlinear relationship between net heat flux and MLD contributes a lot in the mechanisms of SST front weakening. Hereafter, we investigate the MLD responses to the SST front.

To examine how the MLD response to SST front, we matched up daily AMSR-E products with the ship-measured point. The match-up spatial window is 0.125°, time window is within 12 h. Totally, 811 points are derived. Kara et al. (2003) compared several definition methods with the isotherm layer depth, and suggested that the temperature difference $\Delta T = 0.6\,^{\circ}\mathrm{C}$ is suitable in subtropical zone. Therefore, in the present paper we define the MLD as the depth where $T_0 - T_z = 0.6\,^{\circ}\mathrm{C}$.

Scatter plots of SST and MLD are shown in Fig. 8a. Just as we expected, the MLD decreases with the SST increases. The correlation between SST and MLD in front zone is −0.68, their linear relationship suites the function: $y = -4.46x + 156.47$, where y is the MLD, and x is the SST. Note that there are some singular points (within red circle). Through investigating the singular point in the image (Fig. 8b), the singular points stay at the edge of warm filament. It indicates the noises results from the macth-up window, and that the linear relationship between MLD and SST is credible.

4 Summary

We investigate the upper oceanic mixed layer variations from 2003–2009, using satellite altimeter SSH, AMSR-E SST and in situ GTSPP data. We found that:

1. The EOF first mode of SLA could explain the steric component of SSH, it occupies 26.3 % in the subtropical front zone. In the seasonal scale, the SSHA is highest in summer (20 cm) and lowest in winter (−20 cm).

OSD
12, 83–101, 2015

2. During SST front weakening period, the correlation between SLA and SST is 0.76, 0.76, 0.38 in clod zone, frontal zone and warm zone, respectively.

3. MLD decreases as SST increases, with a linear regress relationship $y = -4.46x + 156.47$. This relationship could provide feasibility to retrieval MLD from satellite-derived SST products.

Acknowledgements. This study was jointly supported by National Basic Research Program of China (2013CB956502), National Natural Science Foundation of China (41406043, 41406002), the Fundamental Research Funds for the Central Universities (15lgpy26), and the Strategic Priority Research Program of the Chinese Academy of Sciences (No. XDA11010202). Bo Qiu in Hawaii University and associated Wei Zhuang in SCSIO were thanked for their valuable comments in improving this manuscript. We appreciated Remote Sensing System for their AMSR-E SST data. We also thank NCEP/NCAR products. The data in this paper will be available from the first author or corresponding author upon request after publication, and the users must promise that all data will be used only for scientific research.

References

de Boyer Montegut, C., Madec, G., Fischer, A. S., Lazar, A., and Iudicone, D.: Mixed layer depth over the global ocean: An examination of profile data and a profile-based climatology, J. Geophys. Res., 109, C12003, doi:10.1029/2004JC002378, 2014.

Ducet, N., Le Traon P. Y., and Reverdin, G.: Global high resolution mapping of ocean circulation from Topex/Poseidon and ERS-1 and -2, J. Geophys. Res., 105, 19477–19498, 2000.

Friehe C. A., Shaw, W. J.,Rogers, D. P.,Davidson, K. L., Large, W. G., Stage, S. A.,Crescenti, G. H., Khalsa, S. J. S., Greenhut, G. K., and Li, F.: Air-sea fluxes and surface layer turbulence around a sea-surface temperature front, J. Geophys. Res., 96, 8593–8609, 1991.

Gill, A. E.: Atmosphere-Ocean Dynamics, 342–346, Academic Press, San Diego, Calif., 1982.

Hosoda, K.: A Review of Satellite-Based Microwave Observations of Sea Surface Temperatures, J. Oceanogr., 66, 439–473, 2010.

Isoguchi, O., Kawamura, H., and Kono, T.: A study on wind-driven circulation in the subarctic North Pacific using TOPEX/POSEIDON altimeter data, J. Geophys. Res., 102, 12457–12468, 1997.

Kara, A. B., Rochford, R. A., and Hurlburt, H. E.: Mixed layer depth variability over the global ocean, J. Geophys. Res., 108, 3079, doi:10.1029/2000JC000736, 2003.
Kobashi, F. and Kawamura, H.: Variation of sea surface height at periods of 65–220 days in the subtropical gyre of the North Pacific, J. Geophys. Res. 106, 26817–26831, doi:10.1029/2000JC000361, 2001.
Kobashi, F. and Kubokawa, A.:, Review on North Pacific Subtropical Countercurrents and Subtropical mode waters in ocean circulation and climate, J. Oceanogr., 68, 21–43, doi:10.1007/s10872-011-0083-7, 2012.
Kobashi, F. and Xie, S. P.: Interannual variability of the North Pacific Subtropical Countercurrent: Role of local ocean-atmosphere interaction, J. Oceanogr., 68, 113–126, doi:10.1007/978-4-431-54162-2_9, 2012.
Kobashi, F., Xie, S. P., Iwasaka, N., and Sakamoto, T.: Deep atmospheric response to the North Pacific Oceanic Subtropical Front in spring, J. Clim., 21, 5960–5975, 2008.
Levitus, S.: Climatological Atlas of the World Ocean, NOAA Professional Paper 13, U.S. Department of Commerce, 1982.
Monterey, G. I. and Levitus, S.: Climatological cycle of mixed layer depth in the world ocean, Report, 5 pp., NOAA, Silver Spring, Md, 1997.
Qiu, B.: Large-scale variability in the midlatitude subtropical and subpolar North Pacific Ocean: Observations and causes, J. Phys. Oceanogr., 32, 353–375, 2002.
Qiu, C. and Kawamura, H.: Study on SST front disappearance in the subtropical North Pacific using microwave SSTs, J. Oceanogr., 68, 417–426, 2012.
Qiu, B. and Lukas, R.: Seasonal and interannual variability of the North Equatorial Current, the Mindanao Current, and the Kuroshio along the Pacific western boundary, J. Geophys. Res., 101, 12315–12330, doi:10.1029/95JC03204, 1996.
Qiu, C., Kawamura, H., Mao, H., and Wu, J.: Mechanisms of the disappearance of sea surface temperature fronts in the subtropical North Pacific Ocean, J. Geophys. Res.-Ocean., 119, 4389–4398 doi:10.1002/2014JC010142, 2014.
Small, R. J., deSzoeke, S., Xie, S.-P., O'Neil, L., Seo, H., Song, Q., Cornillon, P., Spall, M., and Minobe, S.: Air-sea interaction over ocean fronts and eddies, Dyn. Atmos. Oceans, 45, 274–319, 2008.
Stammer, D.: Steric and wind-induced changes in TOPEX/POSEIDON large-scale sea surface topography observations, J. Geophys. Res., 102, 20987–21009, 1997.

OSD
12, 83–101, 2015

Sun, C., Thresher, A., Keeley, R., Hall, N., Hamilton, M., Chinn, P., Tran, A., Goni, G., Petit dela Villeon, L., Carval, T., Cowen, L., Manzella, G., Gopalakrishna, V., Guerrero, R., Reseghetti, F., Kanno, Y., Klein, B., Rickards, L., Baldoni A., Lin, S., Ji, F., and Nagaya, Y.: The Data Management System for the Global Temperature and Salinity Profile Programme, in: Proceedings of OceanObs.09: Sustained Ocean Observations and Information for Society (Vol. 2), Venice, Italy, 21–25 September 2009, edited by: Hall, J., Harrison, D. E., and Stammer, D., ESA Publication WPP-306, doi:10.5270/OceanObs09.cwp.86, 2010.

Uda, M. and Hasunuma, K.: The eastward subtropical countercurrent in the western North Pacific Ocean, J. Oceanogr. Soc. Jpn., 25, 201–210, 1969.

White, W. B., Hasunuma, K., and Solomon, H.: Large-scale seasonal and secular variability of subtropical front in the western North Pacific from 1954 to 1974, J. Geophys. Res., 83, 4531–4544, 1978.

Xie, S. P.: Satellite observations of cool ocean-atmosphere interaction, B. Am. Meteor Soc., 85, 195–208, 2004.

OSD

12, 83–101, 2015

Sea surface in northwestern Pacific subtropical front zone

C. Qiu et al.

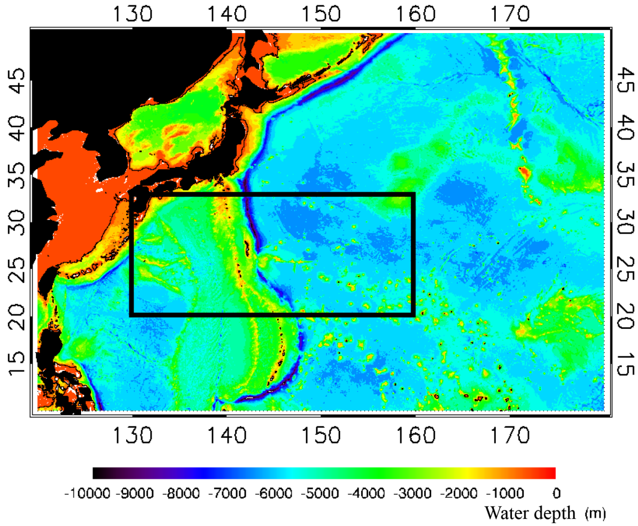

Figure 1. Topography of study area. The black box is the subtropical front zone (Qiu et al., 2014).

OSD
12, 83–101, 2015

Sea surface in northwestern Pacific subtropical front zone

C. Qiu et al.

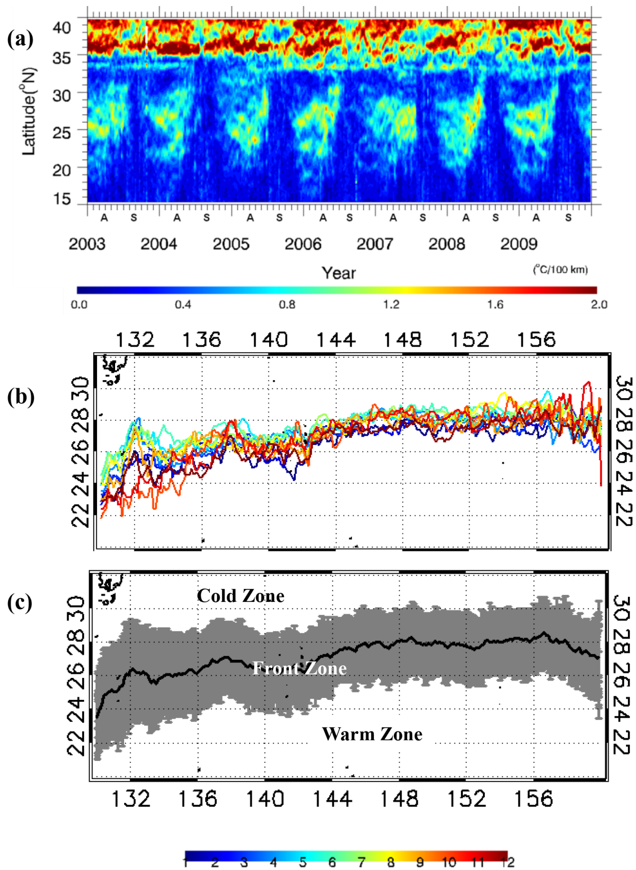

Figure 2. (a) Zonal averaged (130–160° E) sea surface temperature gradient magnitude from January 2003 to December 2009; **(b)** monthly mean frontal position and **(c)** climate mean position with the standard deviations (grey shaded). Color indicates different month. Frontal position is defined as the maximum value of SST gradient magnitude (Qiu et al., 2014).

OSD
12, 83–101, 2015

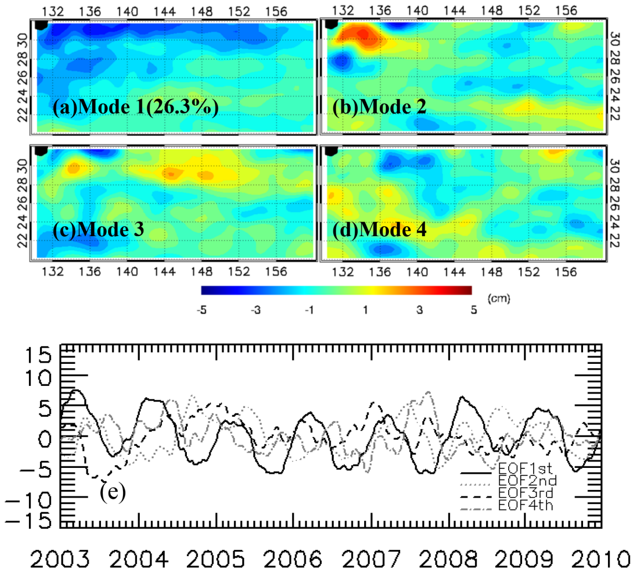

Figure 3. Spatial structure of EOF of SLA **(a)** mode 1st, **(b)** mode 2nd, **(c)** mode 3rd, **(d)** mode 4th, and **(e)** time serials of EOFs. Solid line, dot line, break line, and break dot line are the first mode, second mode, third mode and fourth mode, respectively (Qiu et al., 2014).

OSD
12, 83–101, 2015

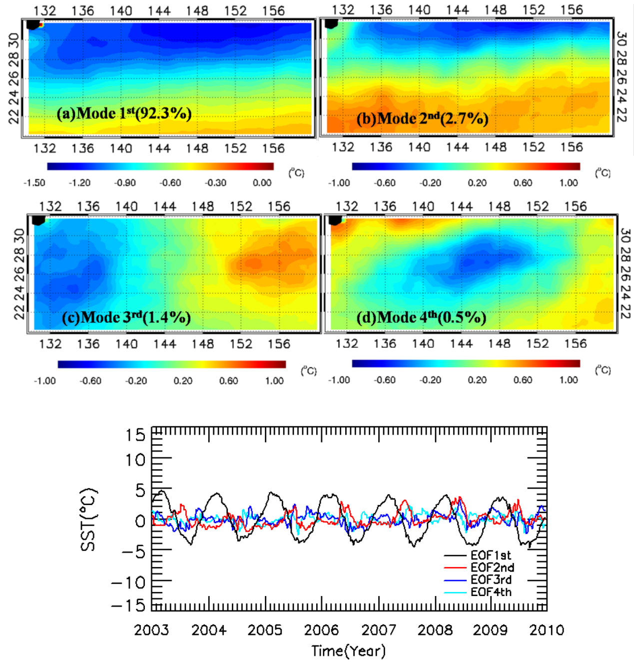

Figure 4. Spatial structure of EOF of SSTA **(a)** mode 1st, **(b)** mode 2nd, **(c)** mode 3rd, **(d)** mode 4th, and **(e)** time serials of EOFs. Solid line, dot line, break line, and break dot line are the first mode, second mode, third mode and fourth mode, respectively (Qiu et al., 2014).

OSD

12, 83–101, 2015

Sea surface in northwestern Pacific subtropical front zone

C. Qiu et al.

Title Page
Abstract | Introduction
Conclusions | References
Tables | Figures
◀| |▶
◀ ▶
Back | Close
Full Screen / Esc
Printer-friendly Version
Interactive Discussion

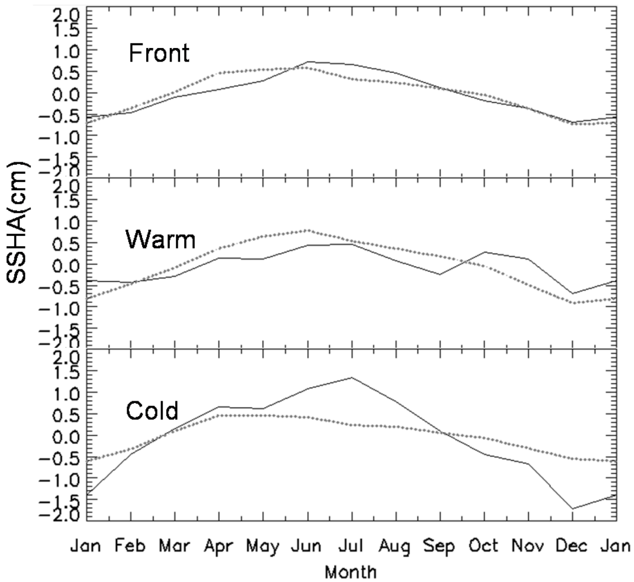

Figure 5. Seasonal variations of SSHA increases (solid line) and steric height increases(dot line) in **(a)** front zone, **(b)** warm zone, and **(c)** cold zone (Qiu et al., 2014).

OSD
12, 83–101, 2015

Sea surface in northwestern Pacific subtropical front zone

C. Qiu et al.

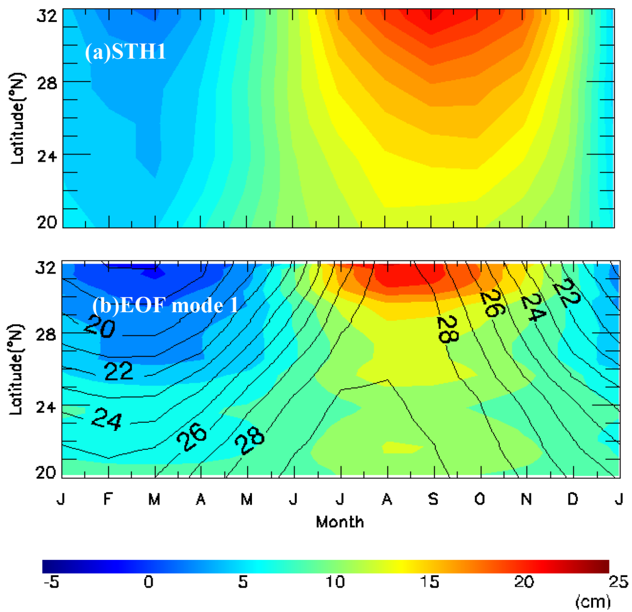

Figure 6. Zonal mean (130–160° E) of seric component of SSHA calculated from **(a)** net heat flux, and **(b)** EOF first mode. The solid line in **(b)** is SST (Qiu et al., 2014).

OSD
12, 83–101, 2015

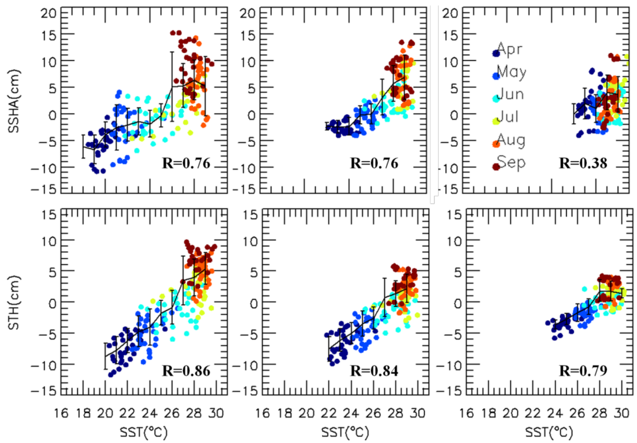

Figure 7. Scatter-plots of **(a)** SST and SSHA, and steric height in cold C front, and warm zone. Color indicates different months from April to September (Qiu et al., 2014).

OSD
12, 83–101, 2015

Sea surface in northwestern Pacific subtropical front zone

C. Qiu et al.

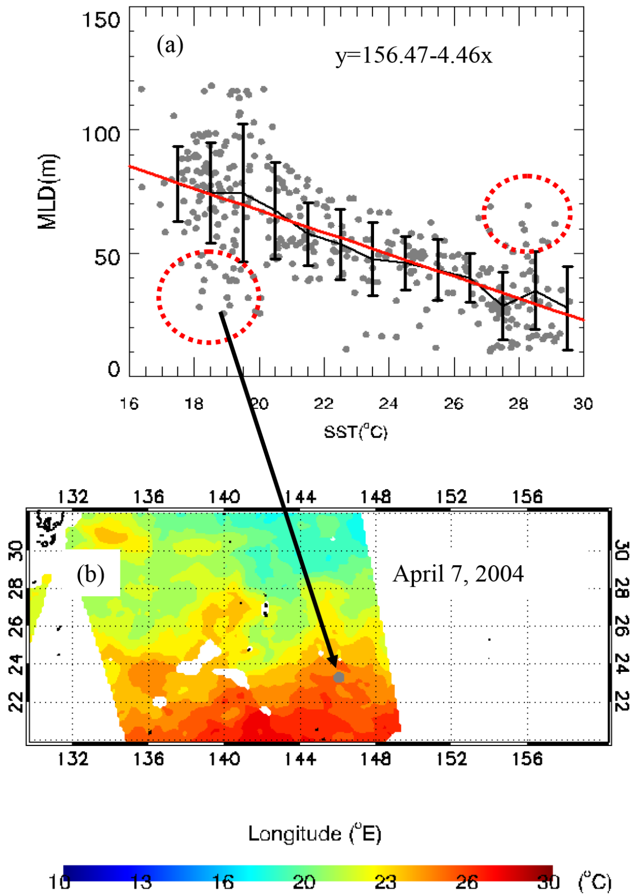

Figure 8. (a) The relationship between SST and MLD in front zone (black dot), and the red circle shows some singular points in warm zone. **(b)** An example of the singular point position and SST distribution on 7 April 2004. The background is SST, and grey dot is the match-up position (Qiu et al.,2014).

OSD
12, 83–101, 2015